

Efficient Quantum Tomography of Two-Mode Wigner Functions

Ludmila A. S. Botelho^{1,*} and Reinaldo O. Vianna¹

¹*Departamento de Física - ICEx - Universidade Federal de Minas Gerais,
Av. Pres. Antônio Carlos 6627 - Belo Horizonte, MG, Brazil - 31270-901.*

(Dated: March 3, 2022)

Abstract

We introduce an efficient method to reconstruct the Wigner function of many-mode continuous variable systems. It is based on convex optimization with semidefinite programs, and also includes a version of the maximum entropy principle, in order to yield unbiased states. A key ingredient of the proposed approach is the representation of the state in a truncated Fock basis. As a bonus, the discrete finite representation allows to easily quantify the entanglement.

PACS numbers: 03.67.-a, 03.65.Wj, 03.65.Ud

arXiv:1912.12222v1 [quant-ph] 27 Dec 2019

*Electronic address: lasb@ufmg.br

I. INTRODUCTION

The Wigner function [1] is a quasi-probability phase space distribution of wide application in diverse areas as quantum physics, quantum electronics, quantum chemistry, and signal processing, to mention a few [2]. In the effervescent field of Quantum Information, it is a tool of paramount importance in the investigation of information processing and quantum entanglement based on continuous variables (CV) [3]. Knowing it is tantamount to the knowledge of the quantum state, which by its turn carries all the information one can know about the quantum system. If one can experimentally reconstruct the Wigner function, by means of Quantum Tomography [4], then the probability distribution associated to the measurement of any property can be predicted.

The first approach introduced to perform the Wigner Function Quantum Tomography (WQT) was based on the inverse Radon Transform [5]. However, besides having a high computational cost, it can yield non-physical functions, equivalent to non-positive density operators, due to imperfect measurements. This last drawback can be corrected by means of Maximum Likelihood approaches (MaxLik) [6]. Notwithstanding, MaxLik can still be impractical due to the high cost of non-linear optimizations. Another difficulty with WQT is that CV quantum states have infinite dimensional Hilbert spaces, therefore one has a quantum tomography scenario that in practice is always informationally incomplete. In this case, the state can not be uniquely determined, *i.e.*, there is a family of states compatible with the available data. In order to single out a state from this family, one can invoke the Maximum Entropy Principle (MaxEnt) [7], which establishes that the least unbiased state is the one that maximizes the information entropy. Combining MaxLik and MaxEnt [8] is a strategy superior to a direct inverse Radon Transform, but is still very computationally demanding. For finite Hilbert spaces, we previously introduced an efficient tomographic approach based on semidefinite programs (SDP), which can handle noisy and informationally incomplete measurements [9–11] in the spirit of the MaxEnt principle [12]. In this paper, we extend our technique to the case of CV states, and show that two-mode states can be reconstructed efficiently with very few measurements and post-processing in low cost desktop computers (say 4 GB and Intel i5 core processor).

The paper is organized as follows. After a quick review of the quantum mechanical description of continuous variable systems, in Sec. II, we introduce our quantum tomography technique in Sec. III. Our approach is illustrated in Sec. IV, where we reconstruct some typical two-mode CV states, and then we conclude in Sec. V.

II. DESCRIPTION OF CONTINUOUS VARIABLE SYSTEMS

A. The Wigner Function

If x is a random variable, according to classical probability theory its characteristic function $\Phi_x(t)$ is the expectation value of $\exp(-itx)$, with t being a real number, namely,

$$\Phi_x(t) = \langle \exp(-itx) \rangle. \quad (1)$$

Out of the characteristic function, we can build the probability density function for x as:

$$F_t(x) = \frac{1}{2\pi} \int_{-\infty}^{+\infty} e^{itx} \Phi_x(t) dt. \quad (2)$$

Now we want to build a probability density function for the position (\hat{q}) and momentum (\hat{p}) operators, which satisfy the usual commutation relation:

$$[\hat{q}, \hat{p}] = i\hbar\mathbb{I}. \quad (3)$$

The characteristic function is formed by the expectation value of an exponential of \hat{q} and \hat{p} analogous to Eq.1, namely:

$$\Phi_{q,p}(u, v) = \text{Tr}(\rho e^{-i(u\hat{q}+v\hat{p})/\hbar}), \quad (4)$$

where u/\hbar and v/\hbar are real numbers, analogous to t , ρ is the quantum state's density matrix, and we used the Born rule to calculate the expectation value. The exponential in Eq.4 is known as the Weyl operator. The probability density function associated to $\Phi_{q,p}(u, v)$, analogous to Eq.2, is the Wigner function [13, 14]:

$$W(q, p) = \left(\frac{1}{2\pi\hbar}\right)^2 \int_{-\infty}^{+\infty} \int_{-\infty}^{+\infty} e^{i(uq+vp)/\hbar} \Phi_{q,p}(u, v) du dv. \quad (5)$$

Notice that q and p are the real values assumed by the position and momentum operators and define the quantum phase space. Using the identity [14]:

$$e^{-i(u\hat{q}+v\hat{p})/\hbar} = \int_{-\infty}^{+\infty} e^{-iuq'/\hbar} |q + \frac{v}{2}\rangle \langle q' - \frac{v}{2}| dq', \quad (6)$$

and after some algebra, we can rewrite the Wigner function in its well known form,

$$W(q, p) = \frac{1}{2\pi\hbar} \int_{-\infty}^{+\infty} \langle q - \frac{v}{2} | \rho | q + \frac{v}{2} \rangle e^{ivp/\hbar} dv. \quad (7)$$

Though $W(q, p)$ yields the correct quantum probabilities,

$$\int_{-\infty}^{+\infty} W(q, p) dp = \langle q | \rho | q \rangle, \quad (8)$$

$$\int_{-\infty}^{+\infty} W(q, p) dq = \langle p | \rho | p \rangle, \quad (9)$$

it is not positive semidefinite, *i.e.*, it is a *quasi-probability* density function. Expectation values of observables (\hat{O}) can be calculated directly from the Wigner function as:

$$\text{Tr}(\rho \hat{O}) = \int_{-\infty}^{+\infty} \int_{-\infty}^{+\infty} W(q, p) O_W(q, p) dq dp, \quad (10)$$

with the Wigner representation of the observable defined as:

$$O_W(q, p) = \int_{-\infty}^{+\infty} \langle q - \frac{v}{2} | \hat{O} | q + \frac{v}{2} \rangle e^{ivp/\hbar} dv. \quad (11)$$

In Classical Physics, expectation values are calculated by means of averages in phase space, and Eq.10 allows us to do an analogous calculation in Quantum Physics.

It is straightforward to re-derive the Wigner function for a system of N particles, and it reads:

$$W(q_1, p_1, q_2, p_2, \dots, q_N, p_N) = \left(\frac{1}{2\pi\hbar} \right)^N \int_{-\infty}^{+\infty} \dots \int_{-\infty}^{+\infty} e^{i(v_1 p_1 + v_2 p_2 + \dots + v_N p_N)/\hbar} \langle q_1 - \frac{v_1}{2}, q_2 - \frac{v_2}{2}, \dots, q_N - \frac{v_N}{2} | \rho | q_1 + \frac{v_1}{2}, q_2 + \frac{v_2}{2}, \dots, q_N + \frac{v_N}{2} \rangle dv_1 dv_2 \dots dv_N. \quad (12)$$

B. The Inverse Radon Transform

Consider the canonical transformation defining the quadratures \hat{q}_θ and \hat{p}_θ :

$$\begin{aligned} \hat{q}_\theta &= \hat{q} \cos \theta + \hat{p} \sin \theta, \\ \hat{p}_\theta &= -\hat{q} \sin \theta + \hat{p} \cos \theta, \\ [\hat{q}_\theta, \hat{p}_\theta] &= [\hat{q}, \hat{p}] = i\hbar. \end{aligned} \quad (13)$$

The probability distribution associated to these quadratures, say

$$pr(q, \theta) = \langle q_\theta | \rho | q_\theta \rangle, \quad (14)$$

can be experimentally determined by means of Homodyne detection [13, 15], and it corresponds to the Radon transform of the Wigner function, namely:

$$\langle q_\theta | \rho | q_\theta \rangle = \frac{1}{2\pi\hbar} \int W(q_\theta \cos \theta - p_\theta \sin \theta, q_\theta \sin \theta + p_\theta \cos \theta) dp_\theta. \quad (15)$$

The Wigner function can then be reconstructed by means of the inverse Radon transform [5],

$$W(q, p) = \frac{1}{2\pi^2} \int_{-\infty}^{+\infty} \int_0^\pi pr(x, \theta) K(q \cos \theta + p \sin \theta - x) dx d\theta, \quad (16)$$

where the integration kernel $K(x)$ is defined as:

$$K(x) = \frac{1}{2} \int_{-\infty}^{+\infty} |\xi| \exp(i\xi x) d\xi. \quad (17)$$

In the case of a single-mode state, the reconstruction is achieved by replacing the kernel $K(x)$ with a regularized numerical approximation, obtained by choosing an appropriate cutoff frequency for the integral in Eq.17. It results in a well known algorithm for image reconstruction, which is not viable for multi-mode states [16], due to technical problems like the very large multi-dimensional grid needed for the inversion, and the difficulty of adjusting the frequency cutoffs for the many modes.

C. Computational Basis and Informationally Complete Measurements

The quantum harmonic oscillator sets the ground for the choice of both the computational basis and Information Complete measurements needed in continuous variable quantum tomography. To simplify notation, from now on we adopt dimensionless operators \hat{q} and \hat{p} , then $\hbar = 1$ and $[\hat{q}, \hat{p}] = i\mathbb{I}$. We start from the annihilation (\hat{a}) and creation (\hat{a}^\dagger) operators, which satisfy the bosonic commutation relation:

$$[\hat{a}, \hat{a}^\dagger] = \mathbb{I}. \quad (18)$$

The dimensionless position and momentum operators, or the quadrature operators, are related to them according to:

$$\hat{q} = \frac{\hat{a}^\dagger + \hat{a}}{\sqrt{2}}, \quad (19)$$

$$\hat{p} = \frac{i(\hat{a}^\dagger - \hat{a})}{\sqrt{2}}. \quad (20)$$

The dimensionless harmonic oscillator Hamiltonian reads (with frequency ω and mass M set to 1):

$$\hat{H} = \hat{a}^\dagger \hat{a} + \frac{1}{2}, \quad (21)$$

and its eigenstates are the number states or Fock states, namely,

$$\hat{a}^\dagger \hat{a} |n\rangle = n |n\rangle. \quad (22)$$

In coordinate representation, a Fock state reads:

$$\langle q|n\rangle = \psi_n(q) = \left(\frac{\alpha}{\pi^{1/2} 2^n n!}\right)^{1/2} \mathcal{H}_n(\alpha q) e^{-\frac{1}{2}\alpha^2 q^2}, \quad (23)$$

with $\alpha = (M\omega/\hbar)$, and \mathcal{H}_n being the Hermite polynomial of degree n .

In contrast to the continuous position and momentum representations,

$$\mathbb{I} = \int_{-\infty}^{+\infty} |q\rangle \langle q| dq = \int_{-\infty}^{+\infty} |p\rangle \langle p| dp, \quad (24)$$

now we have a discrete representation for the CV systems:

$$\mathbb{I} = \sum_{n=0}^{\infty} |n\rangle \langle n|. \quad (25)$$

These three representations are equivalent, and the discrete one is the natural choice for our Computational Basis.

We come then to the last ingredient for our quantum tomography, which is the Informationally Complete basis. With the inverse Radon transform (Eq.5), we learned that the quadratures (Eq.13) form such a basis, namely:

$$\mathbb{I} = \frac{2}{\pi} \int_{-\infty}^{+\infty} \int_0^\pi |q_\theta\rangle\langle q_\theta| dq d\theta. \quad (26)$$

Another Informationally Complete basis is formed by the eigenstates of the non-Hermitian annihilation operator, namely, the coherent states [14]:

$$\hat{a}|z\rangle = z|z\rangle, \quad z = \frac{1}{\sqrt{2}}(q + ip); \quad (27)$$

$$|q, p\rangle \equiv |z\rangle = e^{z\hat{a}^\dagger - z^*\hat{a}}|0\rangle = e^{-|z|^2/2} = \sum_{n=0}^{\infty} \frac{z^n}{\sqrt{n!}}|n\rangle; \quad (28)$$

$$\mathbb{I} = \frac{1}{2\pi} \int_{-\infty}^{+\infty} \int_{-\infty}^{+\infty} |q, p\rangle\langle q, p| dq dp. \quad (29)$$

The probability distributions associated to the informationally complete bases can be experimentally measured by Homodyne detection [15], in the case of quadratures (Eq.26), and by Heterodyne detection, in the case of coherent states (Eq.29) [15, 19].

III. QUANTUM TOMOGRAPHY WITH INFORMATIONALLY INCOMPLETE DATA

Now we take a complete different perspective to the problem of reconstructing the Wigner function. We focus on the quantum state and consider its reconstruction as a matrix completion problem [17]. If some entries of a positive semidefinite matrix is known, it is possible to obtain a low rank approximation to it by means of convex optimization [9, 18]. We first used such idea to estimate entanglement of unknown mixed states [9], and then further developed it to efficient quantum tomography techniques based on semidefinite programs [10–12]. Once the quantum state is obtained, the Wigner function can be calculated by means of Eq.12.

Though we are dealing with CV states and infinite dimensional Hilbert spaces, notice that the computations are always performed with a finite dimensional representation. In the case of the inverse Random transform, for instance, we choose binnings for the quadratures (Eq.13, Eq.14) and cutoffs for the convolutions (Eq.16, Eq.17). Therefore, for the sake of this discussion, we assume a finite dimensional Fock state representation (Eq.25).

Consider a continuous set of informationally complete (\mathcal{IC}) observables ($\{E(\alpha)\}$) forming a positive operator valued measure (POVM), *i.e.*, it expands the density matrix:

$$\int E(\alpha) d\alpha = \mathbb{I}, \quad E(\alpha) \succeq 0. \quad (30)$$

Suppose a few of these observables are actually measured, forming a finite discrete subset ($\mathcal{I} = \{\langle E_i \rangle = f_i\} \subset \mathcal{IC}$), which corresponds to the information we have (\mathcal{I}) about the state. The following SDP reconstructs a unbiased approximation to the quantum state [12]:

$$\begin{aligned}
& \min_{\rho, \Delta_i, \delta} \sum_{i \in \mathcal{I}} \Delta_i + \delta \\
& \text{subject to:} \\
& |\text{Tr}(E_i \rho) - f_i| \leq \Delta_i f_i, \quad \forall i \in \mathcal{I} \\
& \text{Tr} \left(\left(\mathbb{I} - \sum_{i \in \mathcal{I}} E_i \right) \rho \right) \leq \delta, \\
& \Delta_i \geq 0, \quad \forall i \in \mathcal{I} \\
& \delta \geq 0 \\
& \text{Tr}(\rho) = 1, \\
& \rho \succeq 0.
\end{aligned} \tag{31}$$

Minimization of the variational parameters $\{\Delta_i\}$ takes account of the measurement errors associated to the observed frequencies $\{f_i\}$. Minimizing the variational parameter δ forces the probabilities of the non-measured observables ($\langle E_i \rangle \notin \mathcal{I}$) to be the most uniform as possible, as would be required by the Maximum Entropy Principle [7]. The second program line adjusts the estimated state ρ to the observed frequencies. The third program line adjusts the non-measured observables to the MaxEnt principle. Then follows the constraints on the SDP variables, being ρ a positive semidefinite trace one operator, and Δ_i and δ are non-negative real numbers.

IV. APPLICATIONS

In this section, we illustrate the application of our tomographic approach (Eq.31) to typical CV states, chosen based on experimental interest and realizability in the laboratory. The tomographies are performed out of quadratures (Eq.26) or coherent states (Eq.29). The phase space is uniformly sampled, with q (Eq.13) varying from 5 to -5, and θ from 0 to π , in the first case, and z (Eq.28) taken as a real number varying from 0 to 2, in the second case. The computational basis has dimension 11, which corresponds to a finite Fock state representation (Eq.25) truncated at $n = 10$. This choice for n guarantees a numerical precision of 10^{-8} in the expectation values. The calculations were performed using MATLAB ([20]), and MOSEK ([21]) interfaced with YALMIP ([22]) to solve the SDPs.

A. 1-Photon Fock State: Inverse Radon Transform versus SDP

To illustrate the superior efficiency of SDP tomography over the commonly used Inverse Radon Transform (IRT), we reconstructed the one-photon Fock state ($|1\rangle$) (Eq.23), in absence

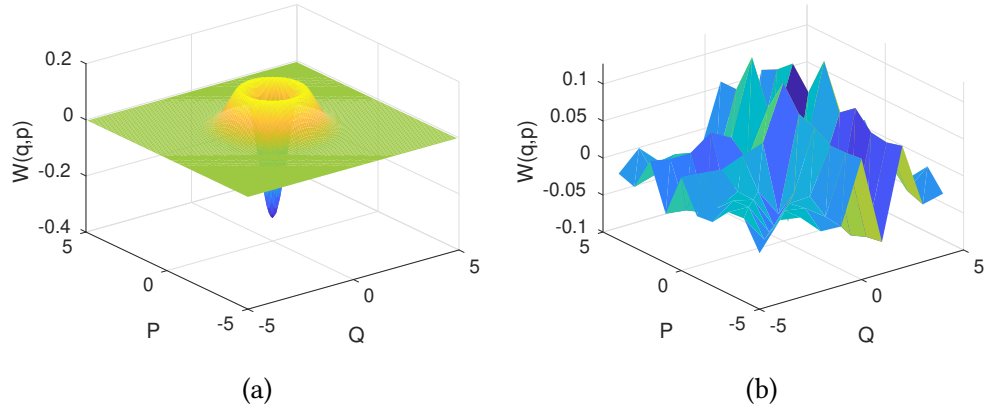


FIG. 1: Wigner Function of the Fock state $|1\rangle$: (a) SDP reconstruction, and (b) Inverse Radon Transform reconstruction with the same amount of measurements.

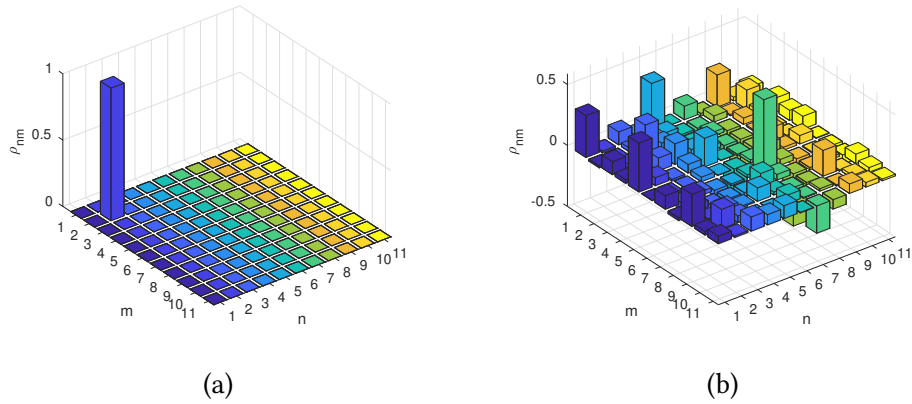


FIG. 2: The density matrix of Fock state $|1\rangle$ reconstructed via (a) SDP, and (b) Inverse Radon Transform (IRT). Notice that the IRT reconstruction resulted in negative values in the diagonal.

of noise. The quadrature operators were uniformly sampled in phase space, taking 7 different values for q , and angles spaced by $\pi/4$ increments, resulting in 35 projectors. This low amount of operators resulted in a perfect reconstruction via SDP (Fig.1a) . The resulting Wigner Function obtained via IRT is shown in Fig.1b. As we can see, with this number of measurements the IRT delivers a very poor result, leading to a non-physical state. In Fig.2, we can see the density matrix reconstructed with the two methods.

B. Two Mode Entangled States

Now we reconstruct four different CV two-mode states, relevant as entanglement resources [23] and also useful in quantum metrology [24]: the NOON state in the Fock basis,

$$|\Psi\rangle_{NOON} = \frac{1}{\sqrt{2}}(|1\rangle_1|0\rangle_2 + |0\rangle_1|1\rangle_2), \quad (32)$$

formed by a one-photon mode and a vacuum mode; the *Hermite-Gauss state*:

$$\Phi(q_1, q_2) = \frac{A_n}{\sqrt{\sigma_+\sigma_-}} \mathcal{H}_n\left(\frac{q_1+q_2}{\sqrt{2}\sigma_+}\right) e^{-\frac{(q_1+q_2)^2}{4\sigma_+^2}} e^{-\frac{(q_1-q_2)^2}{4\sigma_-^2}} \quad (33)$$

where \mathcal{H}_n is the Hermite polynomial of degree n , A_n is a normalization factor and we set $n = 1$, $\sigma_+ = 1$ and $\sigma_- = 0.5$; the *two-mode squeezed vacuum state*, which in position representation reads

$$\Psi(q_1, q_2) = \frac{1}{\sqrt{\pi}} \exp\left[-\frac{1}{4}e^{2\zeta}(q_1+q_2)^2 - \frac{1}{4}e^{-2\zeta}(q_1-q_2)^2\right], \quad (34)$$

while represented in the Fock basis as

$$|\Psi\rangle = \sqrt{1-\lambda^2} \sum_{n=0}^{\infty} \lambda^n |n\rangle|n\rangle, \quad (35)$$

with $\lambda = \tanh \zeta$ and ζ is the squeezed parameter, set to $\zeta = 0.2$; and finally a mixed state in the coherent states basis, the *Dephased Cat*,

$$\rho = N(\alpha, p) \{ |\alpha, \alpha\rangle\langle\alpha, \alpha| + |-\alpha, -\alpha\rangle\langle-\alpha, -\alpha| - (1-p)(|\alpha, \alpha\rangle\langle-\alpha, -\alpha| + |-\alpha, -\alpha\rangle\langle\alpha, \alpha|) \} \quad (36)$$

with $N(\alpha, p)$ a normalization constant, and we set $\alpha = 1$ and $p = 0.5$.

In Fig.3 we show the reconstruction with quadratures, while in Fig.4 the reconstruction is with coherent states. We simulate noisy measurements by means of a Poissonian distribution with 10% signal-to-noise ratio. All the reconstructions needed a small number of measurements, even in presence of noise. A high fidelity to the target state is achieved with about 400 quadratures or 100 coherent states, in all cases.

To check the unbiasedness of the reconstructed states, we randomly chose ten non-measured observables (E_i) and calculated the Shannon entropy of the corresponding probability vector (\vec{p}):

$$S = \sum_{i=1}^{10} -p_i \log_{10} p_i, \quad (37)$$

$$p_i = \text{Tr}[\rho E_i] / N, \quad (38)$$

$$N = \sum_{i=1}^{10} p_i. \quad (39)$$

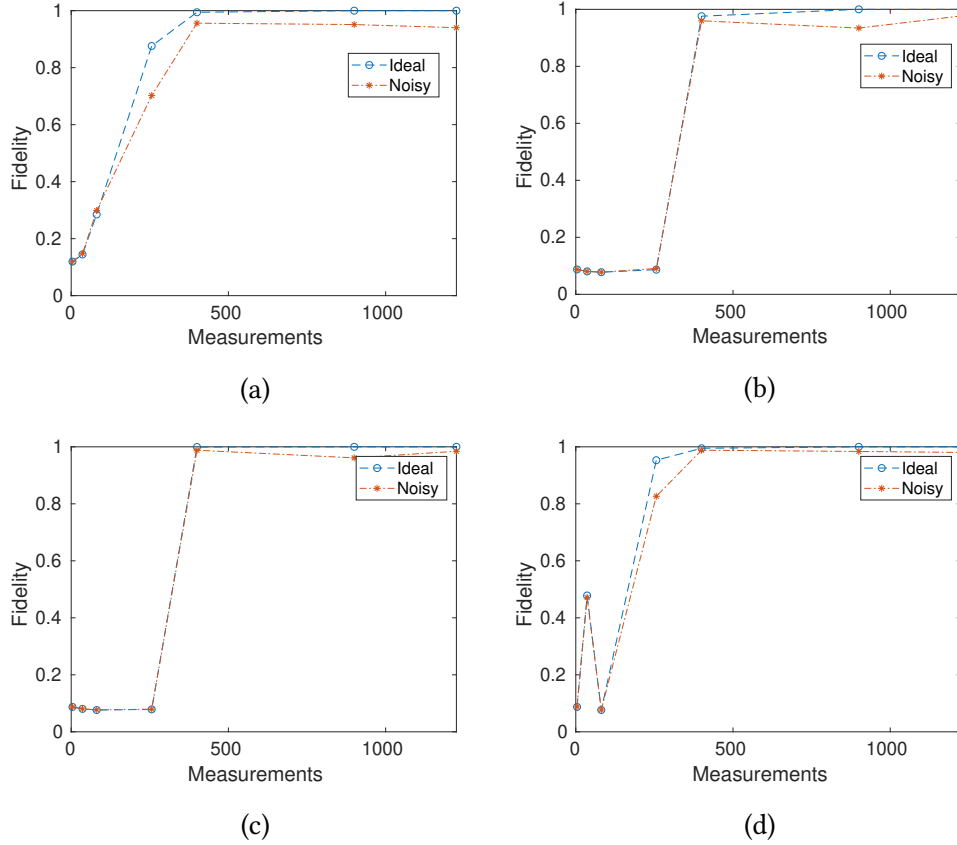


FIG. 3: Fidelity to the target state versus number of measured quadratures: (a) Dephased Cat, (b) Hermite-Gauss, (c) NOON and, (d) Squeezed Vacuum.

The third line of the SDP program (Eq.31) forces \vec{p} to be the most entropic as possible. As an illustration, we compared the entropy for the NOON and Hermite-Gauss states reconstructed, in presence of noise, with ($S_{unbiased}$) and without (S_{biased}) the referred program line. The results show that our reconstruction indeed yields a more entropic state: for the NOON we have $S_{biased} = 0.197$ and $S_{unbiased} = 0.228$, while for the Hermite-Gauss $S_{biased} = 0.333$ and $S_{unbiased} = 0.362$.

In the finite Fock basis representation, it is easy to quantify the entanglement of the reconstructed states, by partially transposing the state (ρ^{T_1}) and calculating the Negativity ([25]):

$$\mathcal{N} = \frac{\|\rho^{T_1}\|_1 - 1}{2}. \quad (40)$$

We obtained $\mathcal{N}(\text{Hermite-Gauss})=0.89$, $\mathcal{N}(\text{NOON})=0.50$, $\mathcal{N}(\text{Squeezed Vacuum})=0.25$, and $\mathcal{N}(\text{Dephased-Cat})=0.24$.

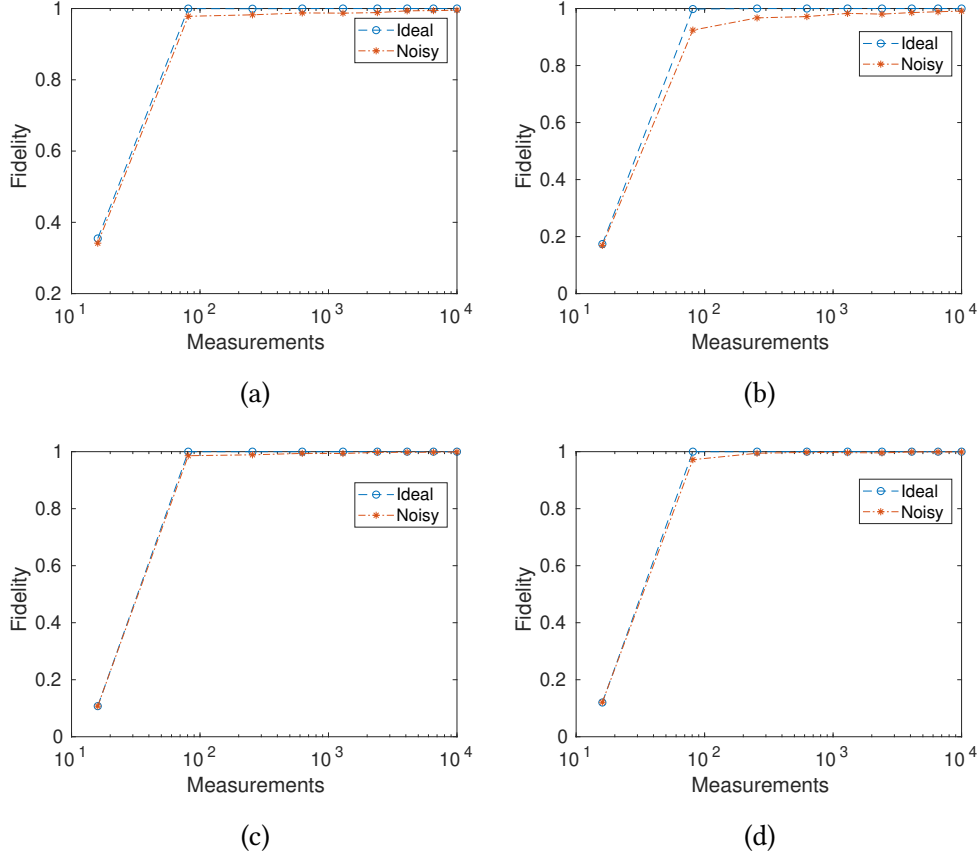


FIG. 4: Fidelity to the target state versus number of measured coherent states: (a) Dephased Cat, (b) Hermite-Gauss, (c) NOON, and (d) Squeezed Vacuum.

V. CONCLUSION

We showed that truncating the Fock basis at number state $n = 10$, it is possible to represent continuous variable states with high numerical precision (10^{-8}) in the expectation values. This discrete Fock basis finite representation allowed us to simulate the reconstruction of two-mode states in a small desktop computer. We introduced a semidefinite program that performs the tomography of the continuous variable states very efficiently in presence of noise, and yields unbiased states in the maximum entropy principle sense. The two-mode states we tested, needed the measurement of about 400 quadratures or 100 coherent states to achieve a high fidelity (> 0.9) reconstruction. By taking advantage of the small finite representation, we assessed the entanglement of the states by means of the negativity.

Acknowledgments

We acknowledge financial support from the Brazilian agencies FAPEMIG, CAPES, and CNPq INCT-IQ (465469/2014-0).

- [1] E. P. Wigner, "On the quantum correction for thermodynamic equilibrium", *Phys. Rev.* 40, 749 (1932).
- [2] J. Weinbub, and D.K. Ferry, "Recent advances in Wigner function approaches", *Appl. Phys. Rev.* 5, 041104 (2018).
- [3] S. L. Braunstein, "Quantum information with continuous variables", *Rev. Mod. Phys.* 77, 513 (2005).
- [4] A. I. Lvovsky, and M. G. Raymer, "Continuous-variable optical quantum-state tomography", *Rev. Mod. Phys.* 81, 299 (2009).
- [5] J. Bertrand, and P. Bertrand, "A tomographic approach to Wigner's function", *Found. Phys.* 17, 397 (1987).
- [6] M. Paris, and J. Rehacek, "Quantum State Estimation", *Lecture Notes in Physics Vol. 649*, Springer, Berlin (2004).
- [7] E. T. Jaynes, "Information Theory and Statistical Mechanics", *Phys. Rev.* 106, 620 (1957).
- [8] V. Buzek, G. Drobny, R. Derka, G. Adam, and H. Wiedemann, "Quantum tomography of Wigner functions from Incomplete Data", *Chaos, Solitons & Fractals* 10, 981 (1999).
- [9] T. O. Maciel, and R. O. Vianna, "Viable entanglement detection of unknown mixed states in low dimensions", *Phys. Rev. A* 80, 032325 (2009).
- [10] T. O. Maciel, A. T. Cesário, and R. O. Vianna, "Variational quantum tomography with incomplete information by means of semidefinite programs", *Int. J. Mod. Phys. C* 22, 1361 (2011).
- [11] T. O. Maciel, and R. O. Vianna, "Optimal Estimation of Quantum Processes Using Incomplete information: Variational Quantum Process Tomography", *Quantum Inf. Comput.* 12, 0442 (2012)
- [12] D. S. Gonçalves, C. Lavor, M. A. Gomes-Ruggiero, A. T. Cesário, R. O. Vianna, and T. O. Maciel, "Quantum state tomography with incomplete data: Maximum entropy and variational quantum tomography", *Phys. Rev. A* 87, 052140 (2013).
- [13] L. E. Ballentine, "Quantum Mechanics, A Modern Development", 2nd Ed., World Scientific, Singapore (2015).
- [14] I. Bengtsson, and K. Życzkowski, "Geometry of Quantum States, An Introduction to Quantum Entanglement", 1st Ed., Cambridge, Cambridge (2008).
- [15] M. J. Collett, R. Loudon, and C. W. Gardiner, "Quantum Theory of Optical Homodyne and Heterodyne Detection", *J. Mod. Opt.* 34, 881 (1987).
- [16] G. Herman, "Image Reconstruction from Projections: The Fundamentals of Computational Tomography", *Computer Science and Applied Mathematics Series*, Academic Press (1980).
- [17] M. Fazel, "Matrix Rank Minimization with Applications", PhD. Dissertation, Stanford University (2002).
- [18] E. J. Candes, and B. Recht, "Exact Matrix Completion via Convex Optimization", *Found. Comput. Math.* 9, 717 (2009).
- [19] U. Chabaud, T. Douce, F. Grosshans, E. Kashefi, and D. Markam, "Building trust for continuous variable quantum states", arXiv:1905.12700 (2019).
- [20] www.mathworks.com

- [21] www.mosek.com
- [22] J. Löfberg, YALMIP : A Toolbox for Modeling and Optimization in MAT- LAB, Proceedings of the CACSD Conference, 2004, Taipei, Taiwan, (unpublished) <http://control.ee.ethz.ch/~joloef/yalmip.php>.
- [23] A. Saboia, F. Toscano, and S. P. Walborn, “Family of continuous-variable entanglement criteria using general entropy functions”, *Phys. Rev. A* 83, 032307 (2011).
- [24] M. W. Mitchell, J. S. Lundeen, and A. M. Steinberg, “Super-resolving phase measurements with a multiphoton entangled state”, *Nature* 429, 161 (2004).
- [25] G. Vidal, and R. F. Werner, “Computable measure of entanglement”, *Phys. Rev. A* 65, 032314 (2002).